Analog Integrated Circuits and Signal Processing (2025) 124:44
https://doi.org/10.1007/s10470-025-02447-4

Electrical analytical approach for hydrogen sensing of $Al_{0.43}Ga_{0.57}As/La_2O_3$: Pt-based CSDG MOSFET

Naveenbalaji Gowthaman[1] · **Viranjay M. Srivastava**[2]

Received: 15 June 2024 / Revised: 15 February 2025 / Accepted: 9 June 2025

Abstract
Nanotechnology has enabled novel sensing approaches with significant potential for environmental monitoring and technological advancements. This research explores the integration of nano-materials in hydrogen sensing, leveraging advanced fabrication techniques to analyze the electrical characteristics of $Al_{0.43}Ga_{0.57}As$ Cylindrical Surrounding Double-Gate (CSDG) Metal-Oxide-Semiconductor Field-Effect Transistors (MOSFETs). The incorporation of nano-materials enhances sensitivity and selectivity, enabling hydrogen gas detection at extremely low concentrations. The sensor maintains a robust response even at elevated temperatures, such as 393 K. The results indicate peak frequencies of 57.36 GHz at 1.105 mA, 56.95 GHz at 1.161 mA, and 56.54 GHz at 1.222 mA for InGaAs (4.6 V), InGaAs (5.0 V), and AlGaAs (1.3 V) configurations, respectively. Thermodynamic analysis reveals hydrogen adsorption enthalpies of approximately −0.58 and −0.19 kJ/mol for DG and CSDG MOSFET devices. This interdisciplinary approach highlights the synergy between nano-material-based hydrogen sensing and fabrication technology, offering a transformative solution for hydrogen detection in industrial processes and emerging energy applications. Furthermore, the strategic implementation of fabrication techniques enhances the precision and reproducibility of sensor devices, ensuring consistent and reliable performance.

Keywords Cylindrical structure · CSDG MOSFET · Dielectric layer · High Electron mobility transistors (HEMTs) · Hydrogen sensing · Hydrogen energy · Microelectronics · Nanotechnology

1 Introduction

This research examines the interaction between nano-material-based hydrogen sensing and the electrical characteristics of $Al_{0.43}Ga_{0.57}As$ Cylindrical Surrounding Double-Gate (CSDG) MOSFETs. By analyzing these characteristics, researchers aim to understand the mechanisms governing hydrogen detection, contributing to advancements in sensor design and practical applications across industrial safety, environmental monitoring, and hydrogen technologies. The integration of advanced fabrication techniques ensures reproducibility, scalability, and enhanced sensor reliability. The cylindrical MOSFET structure is gaining traction for its efficiency in routing, reduced power dissipation, and higher packaging density [1, 2]. The CSDG MOSFETs find applications in mixers, amplifiers, and boost circuits, emphasizing space optimization. However, semiconductor fabrication demands substantial resources, with a single chip requiring 1.6 kg of petroleum and 32 kg of water, contributing to CO_2 emissions and wastewater generation [3–6].

As Ultra-Large-Scale Integration (ULSI) and Very Large-Scale Integration (VLSI) advance, energy consumption increases, exacerbating environmental impacts. Researchers address these concerns by focusing on sustainable hydrogen sensing methodologies using high-speed transistors while aligning their work with the United Nation's (UN) Sustainable Development Goals (SDGs) [7–10]. Addressing this socio-environmental issue, especially in developing countries, achieved some of the UN's goals (SDGs), such as clean water and sanitation (Goal-6), sustainable cities and communities (Goal-11), responsible production and consumption (Goal-12), and life below water (Goal-14),

✉ Viranjay M. Srivastava
viranjay@ieee.org; viranjay.srivastava@bcu.ac.uk

Naveenbalaji Gowthaman
dr.gnb@ieee.org

[1] Department of Computer Science and Engineering, Sri Krishna College of Technology, Coimbatore 641042, India

[2] Department of Electronics Engineering, Birmingham City University, Birmingham B4 7XG, United Kingdom

Published online: 24 June 2025

by 2030. Aligned with SDG's goals this research promotes sustainable technological progress by designing a CSDG MOSFET with improved Short-Channel Effect (SCE) resilience and enhanced observability [11–13]. The fabrication methodology aims to reduce water and energy consumption while maintaining economic viability. Extensive investigations into electrical behavior, including I-V characteristics, saturation, transient responses, and frequency analysis, reinforce the device's potential for hybrid RF applications. This work integrates quantum structures using arbitrary alloys, optimizing MOSFET performance through concentric cylindrical heterostructures [14]. Experimental results reveal a frequency response from 47.89 GHz to 61.77 GHz under a La_2O_3 oxide layer, with distinct voltage kinks at −3 V and 2 V, indicating sensor responsiveness to hydrogen. Testing under a 500 ppm hydrogen environment validates these findings. Additionally, fuel cells are highlighted as key components in clean energy solutions, emphasizing hydrogen's role in power generation [15]. A novel power conditioner architecture featuring Polyphase Boost DC-to-DC converters and Ultra-capacitor-based energy storage enhances energy regulation.

Further research explores hydrogen sensing via co-integrated pseudomorphic doping-channel FETs, demonstrating threshold voltage shifts under hydrogen exposure [16]. Advanced materials such as $Al_{0.43}Ga_{0.57}As$ and La_2O_3 improve sensitivity and selectivity, which is crucial for hydrogen fuel cells and chemical applications [11–15]. The unique CSDG MOSFET gate structure offers heightened sensitivity and faster response times, addressing the growing need for precise hydrogen detection. This work extends prior research [14], emphasizing nanoscale design for scalability, controllability, and environmental sustainability. This paper has been organized as follows. Section 2 details the materials and methodology. Section 3 describes the CSDG MOSFET configuration for Structural fabrication. Section 4 has the fabrication and practical implementation process. Section 5 presents the results with comparative analysis. Finally, Sect. 6 concludes the work and recommends future aspects.

2 Materials employed in CSDG MOSFET design

The Cylindrical Surrounding Double-Gate (CSDG) MOSFETs have gained attention for their potential in semiconductor applications, particularly for sensors. Their integration with La_2O_3 as a dielectric material enhances sensitivity and selectivity, making them highly efficient for detecting hydrogen—a critical component in industrial safety, environmental monitoring, and clean energy applications. The proposed Pt-based CSDG MOSFET for hydrogen sensing in $Al_{0.43}Ga_{0.57}As/La_2O_3$ features a 100 nm gate diameter, 200 nm gate length, and a 20 nm Pt gate atop a 50 nm $Al_{0.43}Ga_{0.57}As$ channel. The 4 nm La_2O_3 gate dielectric ($\varepsilon = 25$) enables hydrogen detection from 1 to 10,000 ppm with a sensitivity of 1 ppm [12]. The sensor exhibits a rapid 10 ms response time and high selectivity, distinguishing hydrogen from methane (100:1) and carbon monoxide (50:1) [14]. It operates across −40 °C to 85 °C and 10–90% relative humidity, with electrical characteristics including a −1.2 V threshold voltage (V_{th}), I_{ON}/I_{OFF} ratio of 10^6, and transconductance of 100 µS.

The device converts voltage to concentration (ppm) as V×0.012 and features a compact 2 mm × 2 mm × 0.5 mm design, weighing 0.1 g. Running on 3.3 V and 5 mA, it withstands radiation up to 10 kRad and industrial gases [13, 14]. With ±1% accuracy and ±0.5% precision, it requires calibration every six months with no routine maintenance. Priced at $100 per unit, this innovation advances hydrogen sensing technology [14–16].

Figure 1 illustrates the Cylindrical Surrounding Double-Gate (CSDG) MOSFET, formed by rotating a double-gate MOSFET around an external axis to create a cylindrical structure. This configuration incorporates $Al_{0.43}Ga_{0.57}As$ with a high-κ La_2O_3 dielectric, optimizing molecular beam

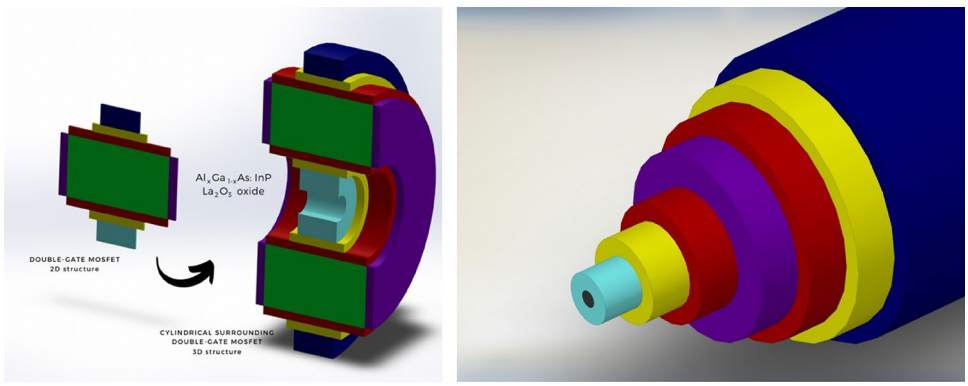

(a) (b)

Fig. 1 (**a**) The CSDG MOSFET (obtained by rotating the DG MOSFET along an external axis) and (**b**) Its diverse layer stacks (isometric view)

epitaxial growth and mitigating Short Channel Effects (SCEs) while enhancing electrical performance [12–14]. The Tellurium (Te) and Palladium (Pd) are optimal dopants, with Pd integrated into the alloy to form the cylindrical heterostructure. The black hue in Fig. 1 represents the central axis around which layers are assembled. Figure 2 shows pre-etching process masks, ensuring design fidelity and structural durability. To withstand electron collisions, a Two-Dimensional Electron Gas (2DEG) layer is incorporated into the core [14]. CSDG MOSFETs offer precise electrostatic control via their gate-all-around architecture, improving sensitivity and reducing power consumption, making them ideal for gas sensing. The La_2O_3, with its high dielectric constant, enhances capacitive coupling, charge sensitivity, and selectivity. Its chemical stability ensures durability in hydrogen-rich environments, while its wide bandgap minimizes leakage current, improving sensor reliability. Surface functionalization further refines hydrogen selectivity, minimizing cross-sensitivity to other gases, crucial for industrial safety and environmental monitoring [14]. The threshold voltage (V_{th}) of the CSDG MOSFET with La_2O_3 dielectric can be expressed as a function of gate-source voltage (V_{gs}), oxide thickness (t_{ox}), and other relevant parameters [12–14]:

$$V_{th} = V_{fb} + 2\phi_f + \frac{Q_{dep}}{C_{ox}} \tag{1}$$

where V_{fb} and ϕ_f are the flat-band voltage and Fermi potential, respectively, and Q_{dep} and C_{ox} are the charges in the depletion region and oxide capacitance, respectively. The drain current (I_d) in the CSDG MOSFET can be described using the basic MOSFET equations, accounting for the threshold voltage, drain-source voltage (V_{ds}), mobility (μ), channel length (L), and other relevant factors [14, 15]:

$$I_d = \frac{1}{2}\mu C_{ox}\frac{W}{L}\left[(V_{gs} - V_{th})\,V_{ds} - \frac{V_{ds}^2}{2}\right] \tag{2}$$

where W is the channel width. The subthreshold swing (S) is a measure of how steeply the transistor turns on and can be given as [11]:

$$S = \frac{dV_{gs}}{d(\log I_d)} \tag{3}$$

The dielectric constant of La_2O_3 can experience changes due to various influencing factors such as temperature and frequency. Its approximation can be established using the Clausius-Mossotti relation [3–5] or the Lorentz-Lorenz Eq. [6]. These equations connect the dielectric constant and the refractive index (n), elucidating the intricate interplay between material properties and electromagnetic characteristics.

$$\frac{\varepsilon_r - 1}{\varepsilon_r + 2} = \frac{N\alpha}{3\varepsilon_0} \tag{4}$$

where N is the number density of atoms or molecules, and ε_0 is the vacuum permittivity constant. Considering the material's molecular polarizability, the Lorentz-Lorenz equation connects the dielectric constant and the refractive index. It is given by,

$$\frac{\varepsilon_r - 1}{\varepsilon_r + 2} = \frac{4\pi N\alpha}{3} \tag{5}$$

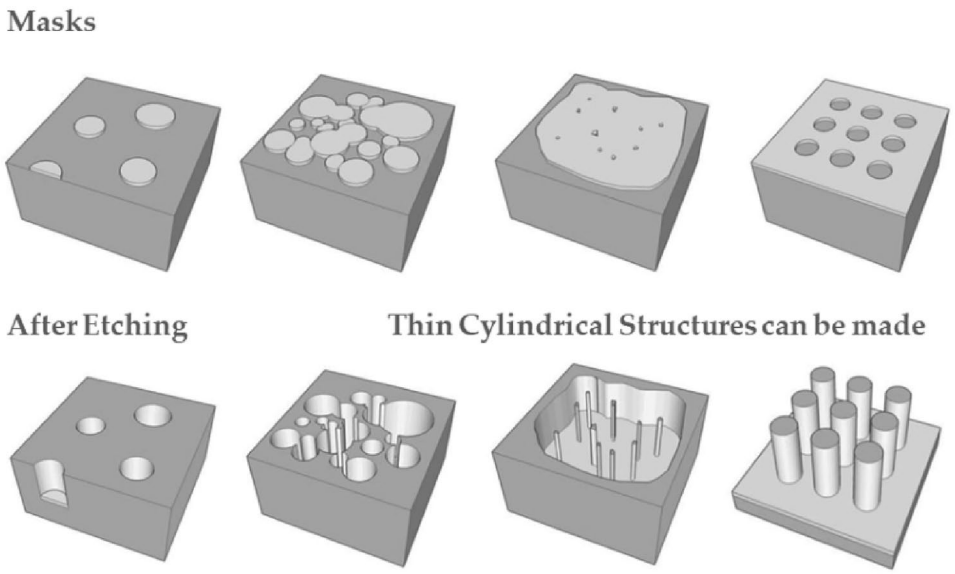

Fig. 2 Diverse mask shapes were devised for the etching procedure [14]

where α is the molecular polarizability. The Lorentz-Lorenz equation provides a more direct way to relate the dielectric constant to the refractive index, incorporating molecular properties. The Clausius-Mossotti relation and the Lorentz-Lorenz equation hold significance in selecting dielectric materials for diverse applications. By linking dielectric constants to molecular properties, these equations enable the prediction of dielectric behavior, aiding material choice based on operating conditions. Their insights into frequency and temperature dependencies guide material selection for varying environments. These equations are used to compare materials, assess dielectric breakdown, optimize optical and RF applications, engineer dielectric properties, and ensure effective insulation. Overall, these equations provide a foundational framework for understanding dielectric behavior, assisting in material selection to enhance the performance of electronic and electrical systems. The surface potential of the CSDG MOSFET is derived from Eq. (3) of ref. [14] by substituting the suitable boundary condition and given as:

$$x = \frac{t_{La_2O_3}}{2} \Rightarrow \psi(x) = \frac{q}{2\varepsilon La_2O_3} N_a \left(\frac{tLa_2O_3}{2}\right)^2 + \frac{2kT}{q} \ln\left|\sec\left(\sqrt{\frac{q^2\eta i}{2\varepsilon La2O_3} e^{\frac{q}{kT}(\psi 0 - V)}} \frac{tLa2O_3}{2}\right)\right| + \psi_0 \quad (6)$$

The surface potential of the CSDG MOSFET with a doped channel has been derived in (6), and it is a function of dopant concentration N_a and potential at the center of the core of CSDG MOSFET ψ_0 [16–18].

The integration of CSDG MOSFETs with La_2O_3 enables real-time and remote hydrogen sensing, leveraging semiconductor compatibility for seamless data acquisition and wireless communication. This capability is crucial for large-scale industrial and remote applications. The gate-all-around architecture, combined with La_2O_3's high dielectric constant and stability, enhances sensitivity, selectivity, and overall performance. As research advances, optimizing fabrication, surface engineering, and system integration will further enhance detection precision and efficiency, addressing critical needs in safety, environmental monitoring, and energy applications [14].

3 CSDG MOSFET configuration for structural fabrication

Gowthaman and Srivastava [14] have highlighted Pt's superiority over conventional metal and Au gate materials, enhancing inner gate controllability. The inner gate (pale blue) is fabricated from Pt, while the gate oxide layer (yellow) consists of La_2O_3, which has a 4.3 eV bandgap—advantageous at the nanometer scale. La_2O_3, composed of Lanthanum and Oxygen, is widely used in ferroelectric devices and catalysis. It has a molar mass of 325.808 g/mol and a solid-state density of 6.51 g/cm³, making it compatible with deposition methods like sputtering, chemical vapor deposition, and atomic layer deposition at 250–450 °C [17]. The spacer layer (red) uses AlAs with a ~ 2.12 eV bandgap, limiting excess charge carrier leakage into the bulk. The bulk layer (purple) consists of $Al_{0.43}Ga_{0.57}As$, with a direct bandgap range of 1.46–2.16 eV, ensuring superior electrical performance [19–22]. The outer gate (royal blue) is also Pt, following the oxide and spacer layers.

For hydrogen sensing, integrating La_2O_3 into CSDG MOSFETs requires precise fabrication. After substrate preparation and gate patterning via lithography, La_2O_3 is deposited using techniques such as Atomic Layer Deposition (ALD) or Physical Vapor Deposition (PVD) [20]. These methods influence film quality, thickness, uniformity, and interface properties, requiring optimization for optimal sensor performance. Hydrogen exposure alters the device's electrical properties, modifying conductance or threshold voltage and enabling concentration quantification [23]. Key performance metrics include sensitivity, selectivity, response time, and recovery time. Figure 1 illustrates the final CSDG MOSFET configuration with the La_2O_3 dielectric, demonstrating its suitability for hydrogen sensing.

Figure 2 illustrates the mask design utilized to achieve the intended material structure post-etching. During the etching process, the exposed layer is targeted, and to construct the cylindrical structure, a small circle with the desired radius is strategically positioned atop the layer.

4 Fabrication and practical implementation

The design of a CSDG MOSFET for hydrogen sensing applications involves several key considerations that leverage the unique features of CSDG architecture and the properties of the chosen dielectric material, such as La_2O_3. The key design parameters of the proposed CSDG MOSFET for hydrogen sensing, including its dimensions, electrical characteristics, and operational specifications, are summarized in Table 1. This design aims to optimize the sensor's sensitivity, selectivity, and response while ensuring compatibility with fabrication processes and potential integration with readout circuits. The fabrication setup equation for CSDG MOSFET involves intricate parameters, techniques, and materials. It can be expressed as:

$$F_{CSDG} = S_{Litho} + S_{Dep} + S_{Etch} + S_{Ip} + S_{Ann} + S_{Test} \quad (7)$$

Table 1 CSDG MOSFET dimensions and key parameters

Parameter	Value	Unit
Gate Diameter	100	nm
Gate Length	200	nm
Pt Gate Thickness	20	nm
Channel Thickness ($Al_{0.43}Ga_{0.57}As$)	50	nm
La_2O_3 Dielectric Thickness	4	nm
Dielectric Constant (ε)	25	–
Detection Range	1–10,000	ppm
Sensitivity	1	ppm
Response Time	10	ms
Selectivity (H_2 : CH_4)	100:1	–
Selectivity (H_2 : CO)	50:1	–
Operating Temperature	−40 to 85	°C
Operating Humidity	10–90%	RH
Threshold Voltage (Vth)	−1.2	V
I_{ON}/I_{OFF} Ratio	10^6	–
Transconductance	100	µS
Voltage-to-Concentration Conversion	V × 0.012	ppm
Device Dimensions	2 × 2 × 0.5	mm
Device Weight	0.1	g
Power Supply	3.3 V, 5 mA	–
Radiation Tolerance	Up to 10	kRad
Calibration Frequency	Every 6 months	–
Accuracy	± 1%	–
Precision	± 0.5%	–
Price per Unit	$100	USD

where F_{CSDG} represents the overall fabrication process for CSDG MOSFET, and S_{Litho} denotes the lithography steps, including photoresist application, exposure, and development. S_{Dep} encompasses deposition techniques for layers like gate, dielectric, and spacer materials, S_{Etch} accounts for etching processes to define various layers and structures, S_{Ip} includes ion implantation for dopants and impurities, S_{Ann} refers to thermal annealing for activation and recovery processes, and S_{Test} encompasses the testing, characterization, and performance evaluation stages. The fabrication steps and design process involved in CSDG MOSFET have been given as follows,

i. **Gate-All-Around (GAA) Architecture**: The primary advantage of CSDG MOSFETs lies in their GAA architecture. This involves surrounding the channel region with gate material on all sides. For hydrogen sensing, this design enhances sensitivity by offering precise control over the channel region and efficient charge modulation [24].
ii. **Material Selection**: Lanthanum Oxide (La_2O_3) is chosen as the dielectric material due to its high dielectric constant (ƙ) and chemical stability [10]. Its ƙ value contributes to strong capacitive coupling, which boosts charge sensitivity, while its stability ensures reliable operation in the presence of hydrogen gas.
iii. **Channel Material**: The semiconductor material used for the channel region impacts the device's performance. Silicon or compound semiconductors like $Al_{0.43}Ga_{0.57}As$ can be considered, balancing factors like electron mobility and charge sensitivity.
iv. **Gate Structure**: Fabrication begins with the substrate's preparation and the gate structure's patterning using lithography. The choice of gate material, thickness, and doping affects the overall device performance and capacitance.
v. **Dielectric Deposition**: The La_2O_3 deposition techniques, such as ALD and PVD, are employed to create a uniform and thin dielectric layer. Optimization of deposition parameters ensures consistent film quality and thickness.
vi. **Surface Functionalization**: To enhance selectivity towards hydrogen gas, the surface of the La_2O_3 layer can be functionalized. This involves modifying the surface chemistry to create specific interactions with hydrogen molecules while minimizing interference from other gases.
vii. **Sensing Mechanism**: The interaction between hydrogen gas and the La_2O_3 layer induces changes in electrical properties, such as conductance or threshold voltage. The sensing mechanism involves measuring these changes and correlating them with gas concentration.
viii. **Integration with Readout Circuitry**: The CSDG MOSFET can be integrated with on-chip readout circuits to facilitate real-time monitoring. These circuits amplify, process, and convert electrical signals into measurable data, allowing for remote monitoring and analysis.
ix. **Calibration and Testing**: The sensor's response to hydrogen gas is characterized under controlled conditions to establish sensitivity, selectivity, response time, and recovery time. Calibration ensures accurate gas concentration determination.
x. **Data Analysis and Interpretation**: Data collected from the sensor has been analyzed to deduce the gas concentration. This can involve mathematical models and algorithms correlating electrical changes with hydrogen concentration.
xi. **Optimization**: Iterative refinement of the design, fabrication techniques, and functionalization strategies is carried out to achieve optimal sensor performance.
xii. **Application Specifics**: Depending on the target application, the sensor's operational parameters, such as detection range, sensitivity, and response time, may need to be fine-tuned. For instance, safety applications might prioritize rapid response times, while industrial processes require high sensitivity at specific concentration ranges.

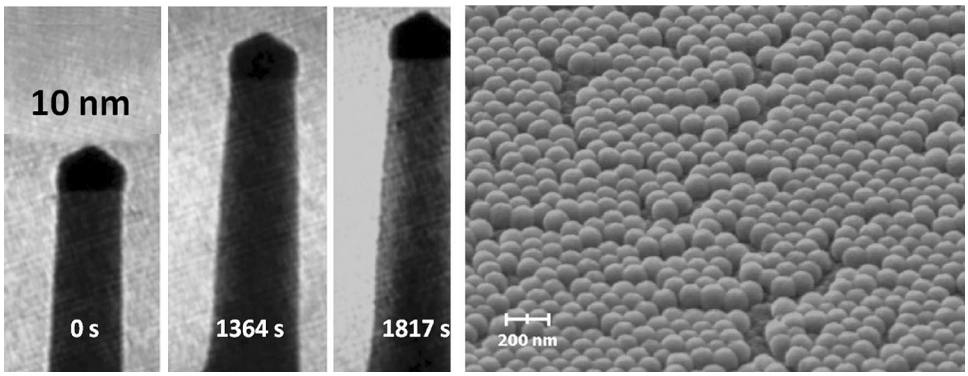

Fig. 3 Growing experimental cylindrical specimens with a diameter of 10 nm involves (**a**) the use of masks and subsequent ion implantation, (**b**) the SEM representation of the nano-bumpy Pd film on the sensing FET within the sensor platform (within the context of the CSDG MOSFET regime) [14, 15]

In summary, designing a CSDG MOSFET for hydrogen sensing with La_2O_3 as the dielectric material involves a holistic approach. It harnesses the strengths of the CSDG architecture and leverages the unique properties of La_2O_3 to engineer a highly sensitive and selective gas sensor. Careful consideration of materials, fabrication processes, surface engineering, and integration with readout circuits collectively contributes to a comprehensive sensing solution with the potential to revolutionize gas sensing technology across various domains.

5 Results and discussions

The simulated device has undergone electrical testing to assess its sensing capabilities on the nanometer scale. Simulation outcomes elucidate the impact of dopants within the chamber upon transistor activation. This research introduces three-dimensional structures, and their outcomes are juxtaposed against planar, DG MOSFET, and traditional systems possessing different lengths. Notably, the observed oscillations demonstrate comparability with conventional sensing methodologies. This work harnesses the virtual cathode principle to ascertain hydrogen concentration. This determination is accomplished via a nanometer-scale, cylindrical heterostructure-based device. Figure 3(a) demonstrates the masks and ion implantation following predetermined timeframes. The evolution of the cylindrical structure is meticulously scrutinized through Transmission Electron Microscopy (TEM) analysis [23, 25, 26]. The experimental setup involved employing a mask with a 10 nm diameter, explored at different time points—0 s, 1364 s, and 1817 s, respectively. The progression of the structure was meticulously observed to gauge its structural integrity and endurance. After the strength assessments, additional layers can be introduced, conforming to specified dimensions as required. Figure 3(b) showcases the SEM depiction of the nano-bumpy Pd film on the sensing FET within the sensor platform under the CSDG MOSFET regime. Notably, a densely arranged nano-bumpy Pd structure is discernible,

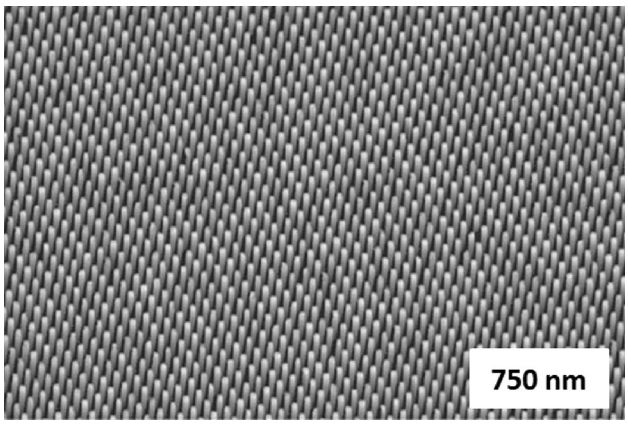

Fig. 4 Individual cylindrical structures are formed for strength testing [14]

being deposited on the template. Impressively, the form of the Pd film remained intact post-heat treatment [27]. This Pd film materialized with bumpy and embossed configurations, encompassing a continuous Pd layer measuring approximately 60 and 50 nm in height. The nano-bumpy Pd structure displayed coherence without any voids, and each cell was seamlessly interconnected with its adjacent counterparts through open channels [28, 29].

Figure 4 depicts the process of creating distinct cylindrical structures, specifically to evaluate their strength characteristics. This step is vital in understanding the structural integrity of the components. The influence of Pt gate thickness on the range of H_2 gas detection is also realized in Fig. 5. In Fig. 5(a), the detection behavior for low H_2 gas concentrations is depicted for the 2 nm gated device. Notably, Fig. 5(b) highlights strong sensing capabilities across H_2 gas concentrations ranging from 2,000 to 30,000 ppm.

Figure 6(a) illustrates the output of the Novel CSDG MOSFET, functioning as a remarkably sensitive current sensor. Utilizing the drain current for sensing provides a precise means to monitor and quantify electrical currents within a common Source-Drain-Gate arrangement. This develops the inherent connection between drain current and flow, allowing accurate assessment in various applications.

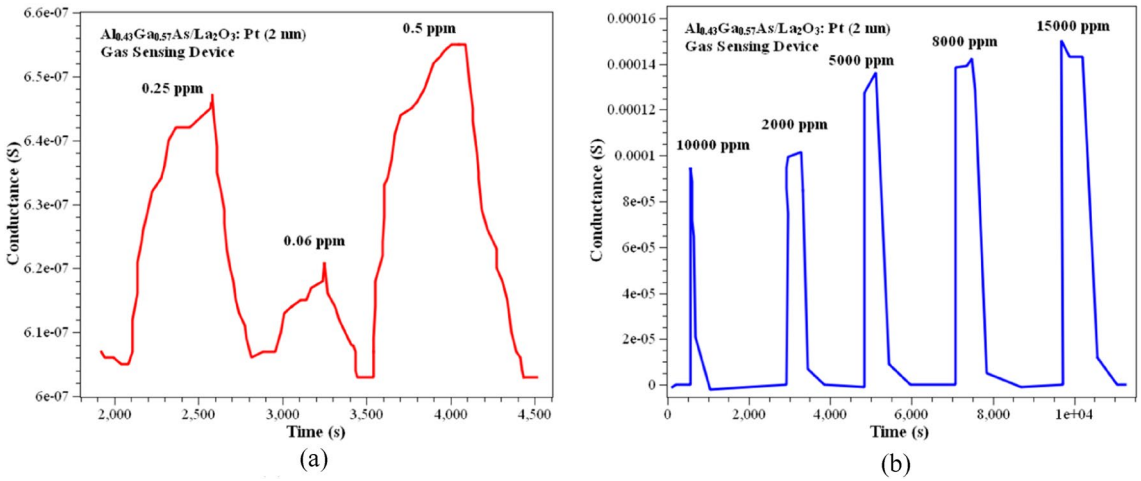

Fig. 5 The gas sensing performance of the CSDG MOSFET device in the presence of (**a**) minimal H_2 concentration and (**b**) elevated H_2 concentration

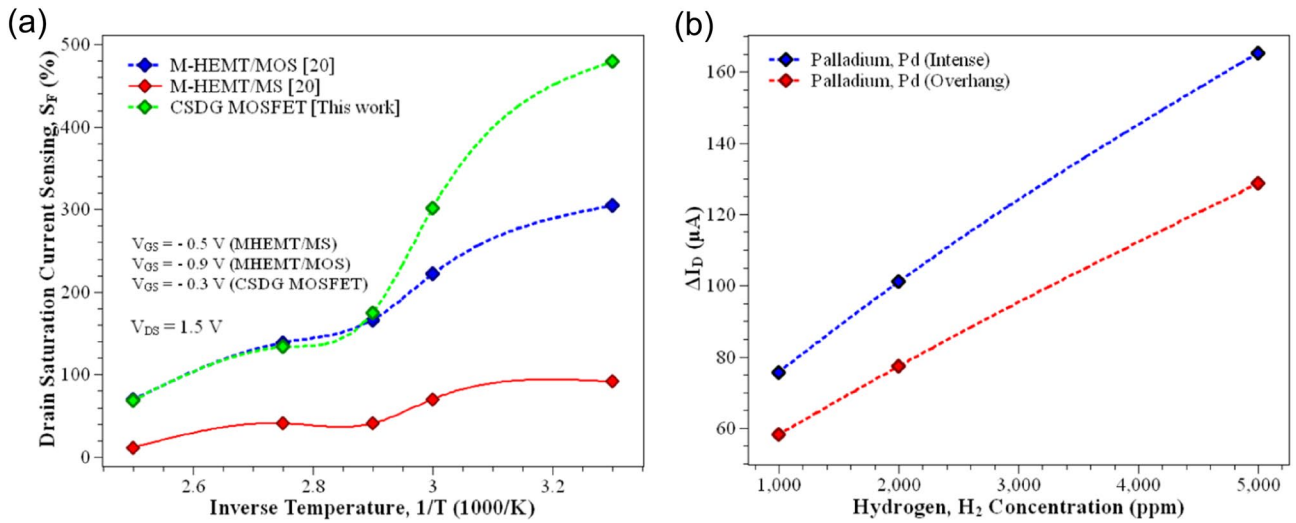

Fig. 6 Novel CSDG MOSFET for current sensing: (**a**) Detection through drain current in a CSDG environment (**b**) Sensing different gas environments using the same device

Table 2 Observations of drain current across various concentrations [15]

Hydrogen concentration (ppm)	I_D, Drain current (mA)	
	Pd (Intense) HEMT	Pd (Overhang) HEMT
1000	75.647	58.117
2000	100.974	77.273
5000	165.264	128.571

With heightened sensitivity and reliability, this mode addresses challenges in precise current measurement, which is vital in electronic systems [12]. Figure 6(b) demonstrates the MOSFET's extension beyond conventional current sensing, enabling the detection of varied gas environments. Designed for this purpose, the device detects alterations in gas properties effectively, as in Table 2. Its unique attributes make it ideal for perceiving changes in gas electrical properties, enhancing its adaptability and impact. In Fig. 6(b), the hydrogen sensing reactions of a heterostructure device are depicted for varying concentrations of Hydrogen gas. When employing an Intense Pd-gated heterostructure, the drain current exhibits fluctuations from 75.647 mA to 165.264 mA, covering the range of 1000 ppm to 5000 ppm. Conversely, an overhang Pd gated heterostructure yields drain current variations of 58.117 mA to 128.571 mA across the same concentration spectrum.

The applied drain-source voltage (V_{DS}) is consistently maintained at 1.3 V. The gate-source voltages for the Metal-HEMT (M-HEMT) exhibit values of 0.5 V and 0.9 V, corresponding to the Metal Oxide Semiconductor (MOS) and Metal Semiconductor (MS) variations, respectively. As temperatures rise within the sensing environment, the value of S_F, the sensing factor, demonstrates an increasing

Table 3 Comparison of drain saturation current sensing across different devices

Inverse temperature, 1/T (1000/K)	Drain Saturation Current Sensing, SF		
	M-HEMT/MOS [16]	M-HEMT/MS [16]	CSDG MOSFET [This work]
2.50	70.01	11.40	68.58
2.55	93.19	23.55	91.72
2.60	116.37	35.70	114.86
2.65	139.55	47.85	138.00
2.70	162.73	60.01	161.14
2.75	185.91	72.16	184.28
2.80	209.09	84.31	207.42
2.85	232.27	96.46	230.56
2.90	255.45	108.61	253.70
2.95	278.63	120.76	276.84
3.00	301.81	132.92	299.98
3.05	324.99	145.07	323.12
3.10	348.17	157.22	346.25
3.15	371.35	169.37	369.40
3.20	394.53	181.52	392.54
3.25	417.71	193.68	415.68
3.30	440.89	205.83	438.82

trend. This phenomenon arises from the exothermic reactions of gaseous hydrogen, readily available for adsorption [30]. Notably, the temperature dependency of M-HEMT/MOS is more pronounced compared to M-HEMT/MS [11, 15]. However, the CSDG MOSFET proves exceptionally promising and amenable compared to these M-HEMT configurations, displaying heightened controllability and temperature dependency improvements [31]. The magnitude of drain saturation current sensing experiences reduction as the temperature is elevated to 1000/K. Table 3 presents a comparative analysis of drain saturation current sensing among different devices. This table compares the drain saturation current sensing performance of various devices. This analysis provides insights into the efficiency and effectiveness of each device's current sensing capabilities.

The data highlights the output peak frequencies and associated current values for different semiconductor materials and voltage settings. The observed peak frequencies indicate the points at which the highest signal strength or resonance occurs. This analysis suggests that semiconductor material and voltage variations influence the peak frequency output. InGaAs exhibit the highest peak frequency, followed by InGaAs with a slightly lower value and AlGaAs with the lowest. Additionally, higher voltages do not necessarily correlate directly with higher peak frequencies, as seen in the case of InGaAs (5.0 V), which has a slightly lower frequency than InGaAs (4.6 V). These findings underline the importance of material properties and voltage

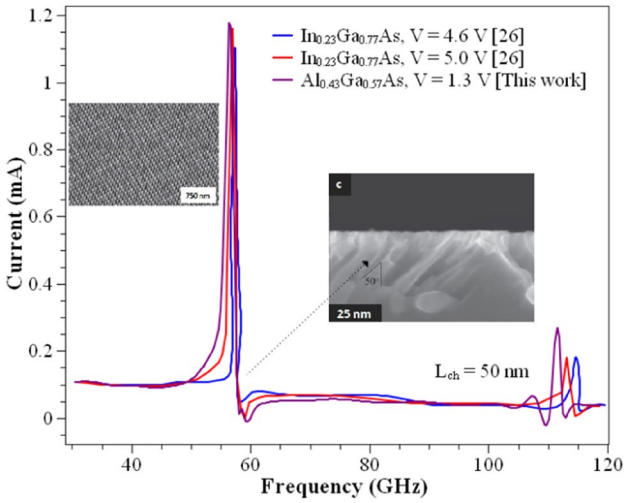

Fig. 7 Amplitude variations in FFT analysis output across devices with diverse nano-materials

considerations in optimizing peak frequency output for specific applications.

Figure 7 depicts amplitude fluctuations in the output of FFT analysis across distinct devices employing diverse nano-materials. The employed materials are varied iterations of arbitrary Indium Gallium Arsenide (InGaAs) alloys. With a notably low bandgap of 0.75 eV between Ge and Si at room temperature, these materials are well-suited for applications in electronics and photodetectors. The previous research reveals output variations under different supply voltages: 4.6 V and 5.0 V for InGaAs, as compared to AlGaAs operating at 1.3 V. The resultant outputs showcase peak frequencies: 57.36 GHz (at 1.105 mA), 56.95 GHz (at 1.161 mA), and 56.54 GHz (at 1.222 mA) for InGaAs (4.6 V), InGaAs (5.0 V), and AlGaAs (1.3 V), respectively. These findings emphasize the impact of supply voltage on the peak frequency output. Notably, InGaAs operate at higher voltages than AlGaAs, yielding higher peak frequencies. This demonstrates the relationship between the supply voltage and frequency response, which is crucial for optimizing device performance. The analysis underscores the significance of voltage settings in influencing semiconductor materials' characteristics and potential applications.

Table 4 reveals that the Pt-based CSDG MOSFET outperforms traditional planar MOSFET sensors in several key aspects. The CSDG MOSFET boasts a notably smaller gate structure (100 nm x 200 nm), which, coupled with its Platinum (Pt) gate material and 20 nm thickness, results in exceptional sensitivity with a minimum detectable concentration of 1 ppm and a broad linear detection range spanning from 1 ppm to 10,000 ppm. It also offers an impressive response time of just 10 milliseconds and remarkable selectivity, favoring Hydrogen (H_2) over other gases at ratios of 100:1 (CH4) and 50:1 (CO). Additionally, it can operate

Table 4 Comparative analysis of Pt-based CSDG MOSFET and traditional planar MOSFET sensors for hydrogen sensing

Parameter	Pt-based CSDG MOSFET	Traditional Planar MOSFET
Gate Structure (Diameter x Length)	100 nm x 200 nm	Larger dimensions
Gate Material	Platinum (Pt)	Silicon dioxide (SiO_2)
Gate Material Thickness	20 nm	Varied
Sensitivity (Minimum Detectable Concentration)	1 ppm	Typically higher ppm
Linear Detection Range	1 ppm − 10,000 ppm	Narrower range
Response Time	10 milliseconds	Slower response time
Selectivity (H_2 vs. Other Gases)	100:1 (CH_4), 50:1 (CO)	Varies
Operating Temperature Range	−40 °C to 85 °C	Varied
Resistance to Radiation	Up to 10 kRad	Varies

over a wide temperature range from − 40 °C to 85 °C and is highly resistant to radiation, withstanding up to 10 kRad. In contrast, traditional planar MOSFET sensors often exhibit higher minimum detectable concentrations, narrower linear ranges, slower response times, and less pronounced selectivity, making the CSDG MOSFET an excellent choice for applications demanding rapid, accurate detection of low hydrogen concentrations, even in challenging environments.

This work encompasses diverse analyses to comprehend the components' structural integrity. The impact of Pt gate thickness on the range of H2 gas detection is explored. The MOSFET functions as an exceptionally sensitive current sensor by utilizing drain current for precise monitoring within a common Source-Drain-Gate arrangement. This sensitivity addresses challenges in accurate, current measurement, which is crucial for electronic systems. It expands the MOSFET's utility by enabling the detection of various gas environments by effectively perceiving changes in gas properties. The materials are iterations of arbitrary Indium Gallium Arsenide (InGaAs) alloys, boasting a low bandgap of 0.75 eV, suitable for electronics and photodetectors. The research extends to Fig. 7, which delves into the relationship between supply voltage and peak frequency output. Notably, InGaAs, operating at higher voltages, yield higher peak frequencies compared to AlGaAs. This highlights the interplay between the supply voltage and frequency response, which is pivotal for optimizing device performance. Overall, the results underscore the profound influence of material properties, voltage settings, and structural considerations in shaping the capabilities and applications of semiconductor devices.

The results cover diverse materials, sensing, and performance topics, showcasing the innovative Novel CSDG MOSFET's potential and contributions to multiple sensing applications and how material properties and voltage settings affect device behavior.

6 Conclusion and future recommendations

This research embodies a conscientious commitment to align with the UN's Sustainable Development Goals, forging a path where technological innovation converges with sustainability, thus advancing industry and responsible production, while contributing to cleaner, more sustainable communities. The amalgamation of a nano-material hydrogen sensing approach with state-of-the-art fabrication technology presents a groundbreaking paradigm in exploring electrical characteristics within $Al_{0.43}Ga_{0.57}As$ CSDG MOSFETs. This research venture combines the realms of nanotechnology, materials science, and semiconductor engineering to deliver a comprehensive understanding of both hydrogen sensing mechanisms and transistor behavior. The outcomes indicate a new era of sensitivity and precision in hydrogen detection by utilizing nano-materials. These innovative materials, tailored at the nanoscale, exhibit exceptional responsiveness to extremely low hydrogen gas concentrations. This sensitivity, coupled with selectivity and rapid response, makes them pivotal in addressing challenges related to hydrogen gas detection in industrial processes, clean energy, and safety applications.

The results demonstrate peak frequencies at 57.36 GHz (with a current of 1.105 mA), 56.95 GHz (with a current of 1.161 mA), and 56.54 GHz (with a current of 1.222 mA) for InGaAs (4.6 V), InGaAs (5.0 V), and AlGaAs (1.3 V) configurations, respectively. In essence, the union of a nano-material hydrogen sensing approach with fabrication technology for analyzing $Al_{0.43}Ga_{0.57}As$ CSDG MOSFETs exemplifies the synergy of multidisciplinary exploration. This convergence pioneers the way for enhanced sensor capabilities and refined semiconductor understanding, fostering solutions to contemporary challenges while opening doors to uncharted technological horizons. Furthermore, this sensor is adept at maintaining a robust sensing response, even under elevated temperatures such as 393 K. Thermodynamic analysis reveals that the enthalpies of hydrogen adsorption for DG and CSDG MOSFET devices are calculated to be approximately − 0.58 and − 0.19 kJ/mol, respectively. The contrasting enthalpy values between these two

analyzed sensors suggest potential divergent mechanisms governing hydrogen adsorption reactions.

Future work will focus on refining nano-material compositions for heightened sensitivity, exploring novel fabrication techniques to enhance device reproducibility, and investigating the potential of integrating AI-driven data analysis for real-time sensing. Moreover, expanding the application scope to other gases and advancing the understanding of transient effects will bolster the practicality and versatility of the nano-material hydrogen sensing approach with fabrication technology, shaping its evolution into a cornerstone of modern sensing technologies.

Acknowledgements Not Applicable.

Author contributions Naveenbalaji Gowthaman (NG) and Viranjay M. Srivastava (VMS) conducted this research, with Conceptualization, methodology, and software validation, NG has designed and analyzed the model with data and wrote this draft article; NG, and VMS validated the figures; VMS verified the result with the designed model; All authors have read and agreed to the published version of the manuscript.

Funding This research received no external funding.

Data availability No datasets were generated or analysed during the current study.

Declarations

Competing interests The authors declare no competing interests.

Ethics approval Not Applicable.

Consent for publication All authors have read and agreed to the published version of the manuscript.

Consent to participate Not Applicable.

References

1. https://irds.ieee.org - International Roadmap for Devices and Systems (IRDS™) 2021 Edition.
2. Naorem, M., Singh, R., & Paily, R. (2021). Detection of Hydrogen Peroxide Using rGO/PPy Nanocomposites in Silicon Dioxide Trench Embedded Field Effect Transistor. *IEEE Sensors Journal, 21*(20), 22426–22433.
3. Kim, S., Yoon, C., Ham, S., Park, J., Kwon, O., Park, D., Choi, S., Kim, S., Ha, K., & Kim, W. (2018). Chemical use in the semiconductor manufacturing industry. *Int J of Occupational and Environmental Health, 24*, 3–4.
4. Hsu, E., Barmak, K., Westabd, A. C., & Park, A.-H. A. (2019). Advancements in the treatment and processing of electronic waste with sustainability: A review of metal extraction and recovery technologies. *Green Chemistry, 21*(5), 919–936.
5. Galbrun-Noel, C. (2022). How semiconductor Fabs can design a greener future? https://blog.se.com/sustainability/2022/01/31/how-semiconductor-fabs-can-design-a-greener-future
6. Karanth, A., Kaya, S., Sikder, A., Carbaugh, D., Laha, S., Tomaso, D. D., Louri, A., Xin, H., & Wu, J. (2019). Sustainability in network-on-chip by exploring heterogeneity in emerging technologies. *IEEE Transactions on Sustainable Computing, 4*(3), 293–307.
7. Awasthi, A. K., Li, J., Koh, L., & Ogunseitan, O. A. (2019). Circular economy and electronic waste. *Nature Electronics, 2*, 86–89.
8. Bhaskar, K., & Kumar, B. (2019). Electronic waste management and sustainable development goals: Is there a business case for linking the two? *Journal of Indian Business Research*, *11*(2), 120–137.
9. Sustainable Development Goals, "About the sustainable development goals". (2018). https://www.un.org/sustainabledevelopment/sustainable-development-goals/.
10. Yong, Y. S., Lim, Y. A., & Ilankoon, I. M. S. K. (2019). An analysis of electronic waste management strategies and recycling operations in Malaysia: Challenges and future prospects. *Journal of Cleaner Production, 224*, 151–166.
11. Srivastava, V. M., Yadav, K. S., & Singh, G. (2011). Design and performance analysis of cylindrical surrounding double-gate MOSFET for RF switch. *Microelectronics Journal, 42*(10), 1124–1135.
12. Maduagwu, U. A., & Srivastava, V. M. (2020). Channel length scaling pattern for Cylindrical Surrounding Double-Gate (CSDG) MOSFET. *IEEE Access, 8*, 121204–121210.
13. Gowthaman, N., & Srivastava, V. M. (2021). Capacitive modeling of cylindrical surrounding double-gate MOSFETs for hybrid RF applications. *IEEE Access*, *9*, 89234–89242.
14. Gowthaman, N., & Srivastava, V. M. (2023). Electrical characteristic analysis of Al0.43Ga0.57As cylindrical surrounding double-gate (CSDG) MOSFET: A nano-material sensing approach with fabrication technology. *International Journal of Hydrogen Energy,* 0360–3199. https://doi.org/10.1016/j.ijhydene.2023.02.059
15. Chandrasekar, V., Chacko, R. V., & Lakaparampil, Z. V. (2011). Design and implementation of an energy-efficient power conditioner for fuel cell generation system. *International Journal of Hydrogen Energy Volume, 36*(22), 15009–15017. https://doi.org/10.1016/j.ijhydene.2011.07.122
16. Tsai, J. H., & Niu, J. S. (2019). Hydrogen sensing characteristics of AlGaInP/InGaAs enhancement/depletion-mode co-integrated doping-channel field-effect transistors. *International Journal of Hydrogen Energy, 44*(3), 2053–2058. https://doi.org/10.1016/j.ijhydene.2018.11.183
17. Moorthy, V. M., & Srivastava, V. M. (2022). Effect of Active Layer Thickness on Organic Thin-Film Transistors. *Ecs Transactions, 109*, 115. https://doi.org/10.1149/10906.0115ecst
18. Moorthy, V. M., & Srivastava, V. M. (2022). Device modelling and optimization of Nanomaterial-Based planar heterojunction solar cell (by varying the device dimensions and material

Parameters). *Nano-materials, 12*(17), 3031. https://doi.org/10.3390/nano12173031
19. Zhang, J., Kosel, T. H., Hall, D. C., & Fay, P. (2008). Fabrication and performance of 0.25 µm gate length depletion-mode GaAs-Channel MOSFETs with self-aligned InAlP native oxide gate dielectric. *IEEE Electron Device Letters, 29*(2), 143–145.
20. Marchi, M. D. (2014). Top-down fabrication of gate-all-around vertically stacked silicon nanowire FETs with controllable polarity. *IEEE Transactions on Nanotechnology, 13*(6), 1029–1038.
21. Li, X. (2011). Vertically stacked and independently controlled twin-gate MOSFETs on a single Si nanowire. *IEEE Electron Device Letters, 32*(11), 1492–1494.
22. Shahrjerdi, D., Rotter, T., Balakrishnan, G., Huffaker, D., Tutuc, E., & Banerjee, S. K. (2008). Fabrication of self-aligned enhancement-mode In0.53Ga0.47As MOSFETs with TaN/HfO2/AlN gate stack. *IEEE Electron Device Letters, 29*(6), 557–560.
23. Convertino, C., Zota, C. B., Caimi, D., Sousa, M., & Czornomaz, L. (2019). InGaAs FinFETs 3D sequentially integrated on FD-SOI Si CMOS with record performance. *IEEE Journal of the Electron Devices Society, 7*, 1170–1174.
24. Forti, V., Blade, K., & Kuehr, R. (2018). *E-waste statistics: Guidelines on classifications, reporting, and indicators* (2nd ed.). United Nations University.
25. Yu, Y. S. (2014). A unified analytical current model for n- and p-type accumulation-mode (junctionless) surrounding gate nanowire FETs. *IEEE Transactions on Electron Devices, 61*(8), 3007–3010.
26. Sallese, J. M., Jazaeri, F., Barbut, L., Chevillon, N., & Lallement, C. (2013). A common core model for junctionless nanowires and symmetric double-gate FETs. *IEEE Transactions on Electron Devices, 60*(12), 4277–4280.
27. Holtij, T., Graef, M., Hain, F. M., Kloes, A., & Iñíguez, B. (2014). Compact model for short-channel junctionless accumulation mode double-gate MOSFETs. *IEEE Transactions on Electron Devices, 61*(2), 288–299.
28. Duarte, J. P., Choi, S.-J., Moon, D.-I., & Choi, Y.-K. (2012). A Non-piece-wise model for long-channel junctionless cylindrical nanowire FETs. *IEEE Electron Device Letters, 33*(2), 155–157.
29. Villa, J., Ramiro, I., Ripalda, J. M., Tobías, I., García-Linares, P., Antolin, E., & Martí, A. (2021). Contribution to the study of sub-bandgap photon absorption in quantum dot InAs/AlGaAs intermediate band solar cells. *IEEE J. of Photovoltaics, 11*(2), 420–428. https://doi.org/10.1109/JPHOTOV.2020.3043855
30. Lee, D. S., Chung, J. W., Wang, H., Gao, X., Guo, S., Fay, P., & Palacios, T. (2011). 245 GHz InAlN/GaN HEMTs with oxygen plasma treatment. *IEEE Electron Device Letters, 32*(6), 755–757.
31. Yoshizawa, H., Huang, Y., Ferguson, P. F., & Temes, G. C. (1999). MOSFET only switched capacitor circuits in digital CMOS technology. *IEEE Journal of Solid-State Circuits, 34*(6), 734–747.

Naveenbalaji Gowthaman (Senior Member, IEEE) received the Bachelors (2011) in Electronics and Communication Engineering, Masters (2013) and Doctorate (2019) in VLSI Design from Anna University, Tiruchirappalli, India. He is currently an Associate Professor in the Department of Computer Science and Engineering (Artificial Intelligence and Machine Learning) at Sri Krishna College of Technology, Coimbatore, India. He has over a decade of academic and research experience in the areas of VLSI design, microprocessors, microcontrollers, and artificial intelligence-based embedded systems. Prof. Gowthaman has authored and co-authored more than 120 technical contributions, including journal articles, conference papers, and book chapters. He co-edited the book Advanced Controllers for Smart Cities – An Industry 4.0 Perspective (Springer Nature, Switzerland AG), which highlights the use of intelligent microcontrollers for large-scale system control in urban environments. His research interests include cylindrical surrounding double-gate MOSFETs, low-power VLSI circuits, VLSI testing, digital electronics, and AI-integrated hardware systems. He is an active member of the IEEE Smart Grid and Smart City Community and the IEEE India Chapter. He is also a life member of ISTE and IETE, and a member of IAENG. He has received several awards, including the Best Teaching Faculty Award (2017), the Innovative Research and Dedicated Teaching Professional Award (2018), the Young Scientist Award (2018), the Outstanding Researcher Award (2018), and the Bright Engineer Award (2019). He serves as an associate editor and reviewer for various peer-reviewed journals, including those published by IET and Springer.

Viranjay M. Srivastava (Senior Member, IEEE) received the Bachelors (2002) in Electronics and Instrumentation Engineering, Masters (2008) VLSI Design, and Doctorate (2012) in RF Microelectronics and VLSI Design. He is currently an Associate Professor with the Department of Electronic Engineering, Birmingham City University, United Kingdom, and Honorary Associate Professor at Howard College, University of KwaZulu-Natal, Durban, South Africa. His research interests include VLSI design, RFICs, analog/mixed-signal IC design, and semiconductor device modeling. Prof. Srivastava has authored/coauthored over 360 scientific publications in peer-reviewed journals and international conferences and has written several academic books in the field. With more than 24 years of teaching and research experience, he has supervised numerous undergraduate, master's, and doctoral theses. His work integrates device fabrication with advanced circuit design to address challenges in energy-efficient and sustainable electronic systems. He is a NRF rated researcher and registered Professional Engineer with ECSA (South Africa), a Life Member of IEEE-HKN, a Senior Member of SAIEE, and a member of IET and IITPSA, Royal Society of South Africa. Prof. Srivastava actively contributes to the IEEE community through paper reviews, conference participation, and technical committees. His interdisciplinary collaborations span academia, industry, and government, supporting innovation and ethical leadership in engineering.